Tension Vector and Structure Matrix Associated Force Sensitivity of a 6-DOF Cable-Driven Parallel Robot

Qinglin Chen[1],[3], Qi Lin [2], Guowu Wei[3], and Lei Ren[4]

Abstract

This paper investigates the force sensitivity of 6-DOF cable-driven parallel robots (CDPRs) in order to propose a better force measurement device. Kinematics and dynamics for a CDPR of *n*-DOF are deduced and formulated, and algorithms for calculating the cable tension are developed. Then, by defining geometrical parameters related to the dimensions and configurations of the CDPRs, optimal methods for determining force sensitivity with respect to the structure matrix and twist vector of the 6-DOF CDPRs with two different moving platforms (i.e. a cubic-shaped, and a flat moving platform) are proposed. By using numerical examples integrated with external twists obtained from wind tunnel tests, numerical simulations and analysis for the two type of 6-DOF CDPRs are carried out. The simulation results help identify the optimal dimensions that can be used to design 6-DOF-CDPR-based force measuring devices with high force sensitivity. Experiment validation is also carried out to verify the method proposed in this paper.

Keywords

Cable-driven parallel robot (CDPR), force sensitivity, force measuring device, structure matrix

Introduction

Cable-driven parallel robots (CDPRs) is a type of parallel robot that is constructed by replacing the rigid limbs (legs) of the traditional rigid-link parallel robot with flexible cables that provide controllable variables for the robots. In recent years, CDPRs have been extensively investigated due to their advantages of producing large reachable workspace, high payload-to-weight ratios, easy disassembly/reassembly, and a light-weight structure; compared with the rigid-link parallel robots. With these advantages, CDPRs have found a broad range of applications in various areas such as space exploration, construction, 3D printing technology, and rehabilitation. These include, to mention but a few, the SkyCam[1] system for high-speed photography tacking; the FAST[2] as a large spherical radio telescope for space exploration and orbit object detection; the RoboCrane[3] for in port cargo carrying, bridge construction and welding; the multiple mobile-crane design for large object transportation[4]; the SPIDERobot[5] for automatic architecture construction; the hybrid-driven-based 3D printer with large workspace for form-based structure printing[6]; the CaTraSys[7] and C-ALEX[8;9] for human working gait tracking, retaining and rehabilitation; the Sophia-3[10] and CAREX[11] for upper limb post-stroke rehabilitation; and the A-TPAD[12] system for improving walking stability of patients with Parkinson's disease. In these applications and development, the associated issues for CDPRs including design and modelling, kinematics and dynamics, control and planning, and structure optimization have been considered, addressed and investigated in certain depth.

Besides the above applications of CDPRs, CDPRs have also been used as a new type of suspension tool for wind tunnel tests[13–15]. In this type of application, it was found that the active cable-driven system can help reduce influence on the air fluent stemming caused by the suspension system, and hence the aerodynamic forces could be directly deduced from the cables tension in the wind tunnel test[16]. However, one of the drawbacks of CDPRs is the driving cables can only apply tensile forces, which means the structure of a cabled

[1] Marine Engineering Institute, Jimei University, Xiamen, China
[2] Department of Aeronautics, Xiamen University, Xiamen, China
[3] School of Science, Engineering and Environment, University of Salford, Salford M5 4WT, UK
[4] Department of Mechanical, Aerospace & Civil Engineering, The University of Manchester, Manchester M13 9PL, UK

Corresponding author:
CHEN Qinglin, Marine Engineering Institute, Jimei University, Xiamen, Fujian Province, 361021, China
Email: cql@jmu.edu.cn

robot will fail to function effectively as long as the cables lose tension. Tension-ability is an essential property for the CDPRs such that all cables need to remain in tension under any external load at the presence of an extra force/impact.

Due to the tension-ability feature, methods for distributing cable tension were proposed to avoid slackness and excessive tension in cables. Abdolshah and Rosati[17] proposed a method by using stiffness, and system dynamics and error values as indices to dynamically change the minimum tension in cables, which led to less power consumption and better performance accuracy. Gouttefarde et al.[18] presented a self-contained and versatile tension distribution algorithm for an *n*-DOF CDPR driven by *n+2* cables, it could process various singularity with the optimal cable tension distributions. Pott[19] proposed an improved force distribution algorithm for CDPRs that could extend the closed-form solution to theoretically maximum wrench-feasible workspace. The improved closed-form solution provides the real-time capability with respect to the workspace (especially near the boundary) while maintaining an acceptable computation time for the implementation in a real-time controller. Boumann and Bruckmann[20] presented an efficient method for calculating cable forces of a CDPR by considering the case that the robot worked outside its wrench-feasible workspace. All the above work is relative to the cable force distribution and is fundamental for CDPRs. Researchers have tried to find out a relatively optimal dimensions for CDPRs when different external loads could be exerted on the moving platform. The investigations also tried to find the effect of a wide range of geometries/dimensions in the proposed CDPRs on the tensile force of each cable in the robot. The instantaneous change of force on each cable is defined as *force sensitivity* of CDPRs.

The sensitivity of force/displacement was studied in some literature. A contact force measurement device was developed for detecting contact force during grasping by describing sensitivity as the relationship between the contact forces and the infinitesimal movement of a parallel platform. Through augmented stiffness matrix, a pair of parameters, which were the distance between the connecting points on the base and moving platform, were derived to simplify the analysis[21].

Another displacement measurement device was designed based on a modified Stewart platform structure and the sensitivity analysis on the device was converted from geometrical characteristics to displacements amplitude. A sensitivity matrix established by 36 parameters presented the performance of each leg when external displacement was applied. Its value increased if the device chose a particular set of geometry, which indicated the best geometry of 6-DOF measuring devices should be calculated before application. However, the sensitivity matrix proposed is too complicated and cannot provide a direct efficient index[22].

When the CDPRs were used as suspension systems of aircraft in wind-tunnel flight testing, the set-up usually permits three rotational degrees of freedom with the bearings providing free roll and pitch, and the yaw motion generated by the cable actuation system. Forces exerted on the moving platform were measured through hydraulic actuators. The research focused on the motion of the moving platform but did not discuss the cable tension sensed by load cells. The work showed the merit of reducing aerodynamic interference by using CDPRs compared with the traditional sting-mounted wind-tunnel testing models[15].

In order to further investigate the advantages of using CDPRs in wind-tunnel flight tests, we proposed a new cable-driven parallel suspension device[13]. With this device, for proof of concept, various of aircraft models were used as moving platform for the tests. The moving platform were driven by eight controllable cables passing through the pulleys mounted on the supporting frame. The cable tension can be measured by force sensor integrated in the cable as shown in Figure 1. The motivation for CDPRs in wind-tunnel flight tests is to make the cable tension change accordingly, and the voltage inside the force sensors could be computed to transfer the aerodynamic force when the incoming flow acts on the supported aircraft model. Through experiments, aerodynamic parameters of the aircraft model are obtained and characterised with the mathematical model that provides the mapping between the readings and the cable tension. However, in most of the cases the tension and its difference on each cable are too small, and hence the test results can be affected by other disturbance such as test errors or the delay of data acquisition.

In order to amplify the difference in the cable tension so as to make it easier to be detected and identified by the force sensors, this paper attempts to provide an improved algorithm based on tension vector and structure matrix from the kinematics and dynamics of the *n*-DOF CDPR. The proposed method can be used to raise the force sensitivity and hence results in a better characterization of the relationship between cable tension and external wrench exerted on the moving platform.

The outline of this article is as follows. The next section describes the modeling of a *m*-cable, *n*-DOF, spatial CDPR including the kinematics, dynamics and distribution of cable tension. The section after presents two kinds of moving platform and the objective to enlarge the force sensitivity.

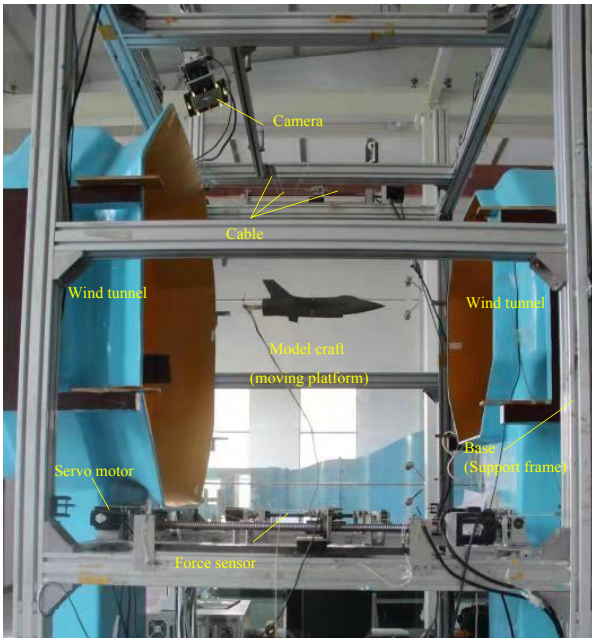

Figure 1. Prototype of the force measuring device.

In the results and discussion, parameterise structure matrix is used to calculate the force sensitivity through algorithms based on the penalty function[23] and the improved close-form method. Experiment validation is also presented to verify the effectiveness and efficiency of the proposed method.

Dynamics of the n-DOF CDPR and Optimization for Cable Tension

Kinematics and dynamics of the n-DOF CDPR

As shown in Figure 1, a 6-DOF CDPR studied in this paper mainly consists of a moving platform and a supporting frame in cubic shape which are connected and actuated by eight cables. For extending the study, kinematics and dynamics of an *n*-DOF CDPRs in a general configuration are deduced. Unlike the traditional rigid-body parallel robot, the general kind of cable-driven parallel robot has incomplete symmetrical configurations of the cables hinged on versatile spindles. The moving platform and the base (supporting frame) are connected by *m* limbs, i.e. *m* cables, integrated with force sensors. When a wrench is exerted on the moving platform, the variation from the force sensors can be used to find the relative position of the moving platform with repect to the fixed base, and correspondingly, to the change of cable lengths.

A schematic diagram of an *n*-DOF CDPR with the associated coordinate systems and wrench is illustrated in Fig. 2. Through *m* cables, the moving platform is connected to the base. Frame {O} represents the global coordinate system attached to the base and frame {P} represents the

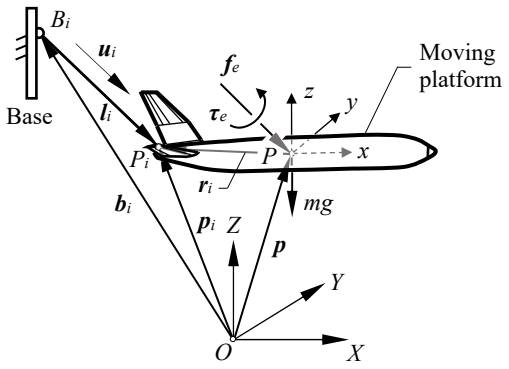

Figure 2. Geometry and wrench of a general cable-driven parallel robot.

local coordinate system attached to the moving platform. The orientation of frame {P} with respect to frame {O} is represented by a rotation matrix $\mathbf{R}$. Vector $\boldsymbol{p} = (X, Y, Z)$ is the position vector of the reference point P presented in the global coordinate system {O}. Orientation of the moving platform with respect to the base is given in a set of $Z - Y - X$ Euler angles α, β and γ making up the set $\boldsymbol{\psi} = (\alpha, \beta, \gamma)$, which can be obtained from a wireless 3D gyro-compass. Thus the pose of the moving platform with respect to the reference frame {O} can be described by $\boldsymbol{q} = (\boldsymbol{p}, \boldsymbol{\psi}) \in SE(3)$. In addition, referring to Fig. 2, vector $\boldsymbol{b}_i = (B_{i,X}, B_{i,Y}, B_{i,Z})(i \in 1, 2, \cdots, m)$ is position vector of the point-shaped hinge for the cable and pulley expressed in the global coordinate system. Vector ${}^p\boldsymbol{p}_i = ({}^p x_{i,x}, {}^p y_{i,y}, {}^p z_{i,z})(i \in 1, 2, \cdots, m)$ is the position vector for a point P_i on the moving platform expressed in the local coordinate system {P}. Both vectors $\boldsymbol{b_i}$ and ${}^p\boldsymbol{p}_i$ are constant in frames {B} and {P}, respectively. $\boldsymbol{p}_i = \boldsymbol{p} + \boldsymbol{r_i}$ is the position vector for a point P_i on the moving platform expressed in the globe coordinate system {O}. Based on all these vectors, the vector that represents the *i*th cable can be written as[24, 25]

$$\boldsymbol{l}_i = \overrightarrow{P_i B_i} = \boldsymbol{b}_i - \boldsymbol{p}_i = \boldsymbol{b}_i - \boldsymbol{p} - \boldsymbol{r_i} \tag{1}$$

where $i = 1, \cdots, m$, and $\boldsymbol{r}_i = \mathbf{R}^p\boldsymbol{p}_i$ is the vector of $\overrightarrow{PP_i}$ expressed in the global reference frame.

From Eq. (1), $\boldsymbol{l}_i$ squared leads to

$$\boldsymbol{l}_i^2 = [\boldsymbol{b}_i - \boldsymbol{p} - \mathbf{R}^p\boldsymbol{p}_i]^T [\boldsymbol{b}_i - \boldsymbol{p} - \mathbf{R}^p\boldsymbol{p}_i] \tag{2}$$

with $i = 1, \cdots, m$.

Taking derivative of Eq.(2) with respect to time and rearranging the equation in matrix form yields[24]

$$\dot{\boldsymbol{L}} = -\mathbf{A}^T\dot{\boldsymbol{q}} \tag{3}$$

where $\dot{\boldsymbol{L}} = [\dot{l_1}, \dot{l_2}, \cdots, \dot{l_m}]$ denotes the velocity vector in the cable length space. $\mathbf{A} = [\boldsymbol{a}_1, \cdots, \boldsymbol{a}_i, \cdots, \boldsymbol{a}_m] \in \mathbb{R}^{6\times m}$ is the structure matrix related to the positions of the moving platform and base, with $\boldsymbol{a}_i = [\boldsymbol{u}_i, \boldsymbol{r}_i \times \boldsymbol{u}_i]^T$ $(i = 1, 2, \cdots, m)$ being the cable vector in which $\boldsymbol{u}_i = \boldsymbol{l}_i / \|\boldsymbol{l}_i\|_2$ is the unit direction vector of the ith cable, where $\|\cdot\|_2$ stands for the Euclidean norm of its vector argument.

$\dot{\boldsymbol{q}} = [\dot{\boldsymbol{p}}^T \quad \dot{\boldsymbol{\psi}}^T]^T = [\dot{X} \quad \dot{Y} \quad \dot{Z} \quad \dot{\alpha} \quad \dot{\beta} \quad \dot{\gamma}]^T$ denotes the Cartesian velocity of the moving platform in $\mathbb{R}^6$ which includes both the linear and angular velocities of the moving platform. The angular velocity can be written as $\boldsymbol{\omega} = \mathbf{H}\dot{\boldsymbol{\psi}}$ with $\dot{\boldsymbol{\psi}} = [\dot{\alpha} \quad \dot{\beta} \quad \dot{\gamma}]$ and

$$\mathbf{H} = \begin{bmatrix} c\beta c\gamma & -s\gamma & 0 \\ c\beta s\gamma & c\gamma & 0 \\ -s\beta & 0 & 1 \end{bmatrix}$$

Referring to Figure 2, the equations of motion[26] for the n-DOF m-cable system expressed in the body-attached frame can be written as

$$\mathbf{A}\boldsymbol{T} = \boldsymbol{W} \tag{4}$$

where $\boldsymbol{T} = [T_1 \quad T_2 \quad T_3 \quad \cdots \quad T_m]^T \in \mathbb{R}^m$ is the vector of cable tensions, $\ddot{\boldsymbol{q}} = [\ddot{\boldsymbol{p}}^T \quad \ddot{\boldsymbol{\psi}}^T]^T = [\ddot{X} \quad \ddot{Y} \quad \ddot{Z} \quad \ddot{\alpha} \quad \ddot{\beta} \quad \ddot{\gamma}]^T$ denotes the acceleration vector in $\mathbb{R}^6$ which includes both the linear and angular acceleration of the moving platform, and $\boldsymbol{W} = -[\mathbf{M}(\boldsymbol{q})\ddot{\boldsymbol{q}} + \mathbf{C}(\boldsymbol{q}, \dot{\boldsymbol{q}})\dot{\boldsymbol{q}} + \mathbf{G}(\boldsymbol{q}) + \boldsymbol{W}_{ext}(\boldsymbol{q})] \in \mathbb{R}^6$ is the wrench exerted on the moving platform.

In the wrench $\boldsymbol{W}$, the term

$$\mathbf{M}(\boldsymbol{q}) = \begin{bmatrix} m_c\mathbf{I}_{3\times3} & \mathbf{0}_{3\times3} \\ \mathbf{0}_{3\times3} & \mathbf{H}^T\mathbf{I}_G\mathbf{H} \end{bmatrix}$$

is the mass inertia matrix, m_c is the mass of the moving platform, $\mathbf{0}_{3\times3}$ and $\mathbf{I}_{3\times3}$ are the zero matrix and identity matrix, $\mathbf{I}_G$ is the 3×3 inertia tensor of the moving platform about point P in frame {P}, the term

$$\mathbf{C}(\boldsymbol{q}, \dot{\boldsymbol{q}})\dot{\boldsymbol{q}} = \begin{bmatrix} \mathbf{0}_{3\times3} \\ \boldsymbol{\omega} \times (\mathbf{I}_G\boldsymbol{\omega}) \end{bmatrix}$$

is the centrifugal and Coriolis force vector,

$$\mathbf{G}(\boldsymbol{q}) = \begin{bmatrix} m_c\boldsymbol{g} \\ \boldsymbol{c} \times m_c\boldsymbol{g} \end{bmatrix}$$

is gravitational vector, $\boldsymbol{g} \in \mathbb{R}^3$ is the gravity acceleration vector, $\boldsymbol{c} \in \mathbb{R}^3$ is the position vector of the centre of mass of the moving platform, and

$$\mathbf{W}_{ext}(\boldsymbol{q}) = \begin{bmatrix} \boldsymbol{f}_e \\ \boldsymbol{\tau}_e \end{bmatrix}$$

is the external wrench, where $\boldsymbol{\tau}_e$ and $\boldsymbol{f}_e$ represent the external moment and force exerted to at point P of the moving platform, respectively.

Based on Eq. (4) and considering the case that the platform is subjected to only the gravity and cable tension, the static equilibrium equation can be given as

$$\mathbf{A}\boldsymbol{T}_0 = -\boldsymbol{G}(\boldsymbol{q}) \tag{5}$$

where $\boldsymbol{T}_0 = [T_{0,1} \quad T_{0,2} \quad T_{0,3} \quad \cdots \quad T_{0,m}]^T \in \mathbb{R}^m$ is the spatial force system of the cable tension to balance the gravity.

Another situation is the moving platform has no linear and angular accelerations due to low velocity with neglect of inertia effect of the moving platform, but there exits an external wrench $\boldsymbol{W}_{ext}$, in this case it has

$$\mathbf{A}\boldsymbol{T}_w = -\boldsymbol{G}(\boldsymbol{q}) - \boldsymbol{W}_{ext}(\boldsymbol{q}) \tag{6}$$

where $\boldsymbol{T}_w = [T_{w,1} \quad T_{w,2} \quad T_{w,3} \quad \cdots \quad t_{w,m}]^T \in \mathbb{R}^m$ is the spatial force system of the cable tension to balance the gravity and the external wrench. As a force measurement device, the purpose is to test the external wrench $\boldsymbol{W}_{ext} = [\boldsymbol{f}_e^T \quad \boldsymbol{\tau}_e^T]^T$ which can be derived through subtracting Eq. (6) from Eq. (5) as

$$\boldsymbol{W}_{ext} = [\boldsymbol{f}_e^T \quad \boldsymbol{\tau}_e^T]^T = \mathbf{A}(\boldsymbol{T}_0 - \boldsymbol{T}_w) = \mathbf{A}\Delta\boldsymbol{T} \tag{7}$$

Obviously, if the difference $\Delta\boldsymbol{T} = \boldsymbol{T}_0 - \boldsymbol{T}_w$ is very small and close to zero, there will be difficulty to test the external wrench, which may cause the force measurement device to lose its functionalities. Also, it should be noted that the derivation of Eq. (7) assumes that the additional wrench does not deform the system, i.e. the additional wrench does not change the geometric structure of the cabled robot and structure matrix $\mathbf{A}$ is assumed to be constant, which means the moving platform should hold at the same position in the whole process of control. For keeping the position, the inverse kinematics delivers the corresponding tendon lengths described as position of the platform, usually this is available from sensors, and the feedback control is used to guide the platform, especially for low speed cases[27;28]. As a solution to this problem, this paper proposes the force sensitivity through the detection of compromising dimensions with

difference $\Delta \boldsymbol{T}$ and structure matrix of the cable-driven parallel mechanism.

Algorithms for calculating the cable tension of the n-DOF CDPR

Comparing with the rigid link, CDPRs require additional actuator to make cables not loose because of the unilateral pulling performance of cables, which means the number of cables, m, required to drive a n-DOF CDPM is at least n+1, i.e. $m \geq n+1$ [29]. For 6-DOF CDPRs, driving the platform with n+2=8 cables rather than with n+1=7 cables leads generally to a larger workspace. It also makes the integrate of the robot into a workshop or a warehouse easier since symmetric cable arrangements in a cuboid supporting frame can be used. Therefore, 6-DOF CDPRs driven by eight cables are common in many applications and this paper also focuses on the redundantly actuated CDPRs driven by n+2=8 cables [18]. The additional cable tension results in a non-trivial null space for the n by m structure matrix. For each pose of CDPRs, the solutions for balancing the cable tension are infinite. The solutions of cable tension, which should be calculated by feasible algorithm, must maintain the cable tension and stay between the upper and lower limits. The upper limit for cable tension is determined by the torque capacity of the actuators, the maximum load limit of cables and the requirement of control. The lower limit for cable tension is a positive magnitude for enduring an unpredictable flab.

Generally, the feasible algorithm for cable tension is fundamentally and broadly studied and its objective function can be differed from the 1-norm [30;31] to ∞-norm [32], but these wide range of choices are inclined to interruption cable tension when the moving platform is expected to contract the desired trajectory [31]. Hence, the p-norm should be more than 1 and no greater up to ∞, particularly the 2-norm has the various merits [33] to compute such optimal tension distributions. With regard to the workspace coverage while maintaining an acceptable computation time for usage in a real-time controller, one of the algorithms can achieve but might only work for robot with arbitrary degree-of-redundancy. Depending on the CDPR type (suspended or fully constrained) and on the required characteristics (real-time capable or continuous solution for control), the desired cable tension distribution is not always the same.

In terms of Eq. (7), the value of $\Delta \boldsymbol{T} = \boldsymbol{T}_0 - \boldsymbol{T}_w$ will change with the different structure matrix $\mathbf{A}$ as long as the additional wrench $\boldsymbol{W}_{ext}$ keeps constant. There are two approaches for getting close relationship for the sensitivity between the $\Delta \boldsymbol{T} = \boldsymbol{T}_0 - \boldsymbol{T}_w$ and structure matrix $\mathbf{A}$. One is by getting the force sensitivity from the various $\Delta \boldsymbol{T} = \boldsymbol{T}_0 - \boldsymbol{T}_w$ through parameterize structure matrix $\mathbf{A}$ with the same feasible algorithm for cable tension. The cubic structure of moving platform would be applied to the analysis for most of the existing CDPRs commonly have this shape, which would be discussed in the next section. The other is by getting the force sensitivity from the various $\Delta \boldsymbol{T} = \boldsymbol{T}_0 - \boldsymbol{T}_w$ through two different optimal algorithms for cable tension with the same dimension of the moving platform. All the connections between the moving platform and the base are in the identical plane which also would be discussed in the next section. Any of the above effective solution should satisfy Eq. (4) and two of them are selected to demonstrate the methods for finding out the factors that influence the force sensitivity of the CDPRs.

According to the penalty function method [23], a non-linear optimization problem can be formulated to find the minimize of cable tension of CDPRs as

Minimize

$$\sqrt{(T_1 - T_{min})^2 + (T_2 - T_{min})^2 + \cdots + (T_m - T_{min})^2}$$

$$\mathbf{s.t.} \begin{cases} T_{\min} \leq T_i \\ \mathbf{A}\boldsymbol{T} = \boldsymbol{W} \end{cases}$$

where $T_{\min}$ is an initial parameter for the optimization, the variables to be optimized are the elements of structure matrix including $\boldsymbol{u}_i (i = 1, 2, \cdots, m)$ and $\boldsymbol{r}_i (i = 1, 2, \cdots, m)$. Based on the penalty function method, it can find the smooth and continuous force for control but it needs more time to complete the iterations compared to the improved closed-form method. In the experiment, the force from the penalty function method should be calculated and distributed in advance. The above objective function and constraints are bound by the following equation,

Minimize

$$\sqrt{\sum_{i=1}^{m} (T_i - T_{\min})^2} + \lambda \left\{ |\mathbf{A}\boldsymbol{T}_i - \boldsymbol{W}|^2 + \sum_{i=1}^{m} \min [T_i, T_{\min}]^2 \right\}$$

where λ is the coefficient for the penalty function method, which can make the acceleration of the calculation to find the minimum and feasible tension.

According to another optimal algorithm, the improved closed-form [19], a non-linear optimization problem can be formulated to judge the minimum cable tension as

Minimize $\sqrt{\sum_{i=1}^{m} {T_i}^2}$

$$\text{s.t.} \begin{cases} \frac{1}{2}T_m \le T_i \le \frac{\sqrt{2}+1}{2}T_m \\ T_m = \frac{1}{2}(T_{\min} + T_{\max}) \\ \mathbf{AT} = \boldsymbol{W} \end{cases}$$

where $T_{\max}$ is the maximum cable tension and an initial parameter for the optimization, the variables to be optimized are the elements of structure matrix including $\boldsymbol{u}_i (i = 1, 2, \cdots, m)$ and $\boldsymbol{r}_i (i = 1, 2, \cdots, m)$. Based on the closed-form and the improved closed-form algorithm, the above objective function can help to find the upper value close to medium which can enlarge the value of $\Delta \boldsymbol{T}$, although there is no formal proof that it holds true in general.

Sensitivity Analysis of 6-DOF CDPRs with Various Configurations

The main objective of this section is to identify how the relationship between the different magnitude of external forces and the geometry configurations affect the sensitivity of CDPRs. Two different configurations, i.e. a CDPR with a cubic-shaped moving platform and a CDPR with a flat moving platform are considered in the analysis.

CDPR with a cubic-shaped moving platform

As mentioned in the previous section, commonly, eight cables were used in a CDPR so as to obtain a larger workspace and symmetrical control[34]. With eight cables, though a specified device with a cubic-shaped moving platform has limitation in angular workspace that the orientation angle is of no more than 40 degree, there is no necessity to set cross cables[35]. For a CDPR with a cubic-shaped moving platform driven by eight cables, it has 16 adjustable points, eight attaching points on the moving platform and eight points at the pulleys mounted on the supporting frame as shown in Figure 3. Each of these points can change the structure matrix $\mathbf{A}$ independently. Hence, there are 48 parameters, each cable gives three position coordinates, and three orientation angles of the moving platform, that can together determine the force sensitivity of the robot. Moreover, the robot is supposed to be symmetrically configured, for simplicity, with regard to the X-Z plane, in such case the number of parameters can significantly decrease to 24. Explicitly, the x, y and z coordinates of the positions of the eight points denoted as $\boldsymbol{P}_1$ throughout $\boldsymbol{P}_8$ have 24 parameters.

Accordingly, using the rig presented in Figure 3, five geometrical and physical parameters of the robot are taken into consideration for the experimental tests. Related to the positions of the eight points, three of the geometrical

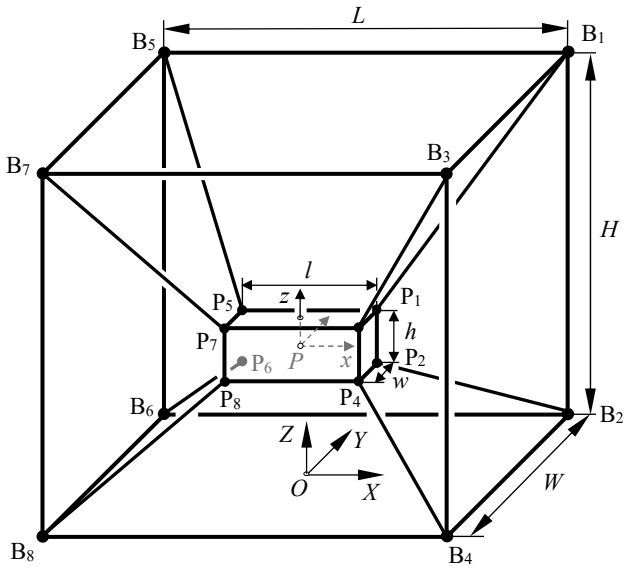

Figure 3. A 6-DOF CDPR with a cubic-shaped moving platform.

parameters are the length ratios between the supporting frame and the cubic-shaped moving platform denoted as k_1, k_2, k_3. Here k_1 stands for the ratio between length l of the moving platform and length L of the supporting frame as $k_1 = l/L$, k_2 is the ratio in the width direction as $k_2 = w/W$ with w being the width of the moving platform and W being the width of the supporting frame, and k_3 the ratio in the height direction as $k_3 = h/H$ with h and H being heights of the moving platform and the supporting frame, respectively. The other two geometrical and physical parameters of the robot are the mass m_c of the moving platform and the position vector $\boldsymbol{p}$ denoting the original point P of the moving platform, which are also importantly found out to affect the force sensitivity. For simplicity but no changing the general purpose, the variation of the original position of point P only allows to change the coordinate value Z, keeping the other 2 coordinate value constant. The four geometric parameters above are gathered as

$$k_1 = l/L, k_2 = w/W, k_3 = h/H, \boldsymbol{p} = [X, Y, Z]^T$$

The range of the proportion k_i $(i = 1, 2, 3)$ makes the dimension of quadrangle variable, which is formed by two cables and two solid links as shown in Figure 3. The proportion k_i shifts from 0.025 to 0.5 in order to change the dimension of the quadrangles in terms of the applications. The dimension of the moving platform will be equal to that of the base if $k_i = 1$ $(i = 1, 2, 3)$. Generally, the geometrical configurations of moving platform or the base is confirmed by the condition of measurement. Accordingly,

the proportion k_i is set to be less than 0.4. Parameters of the vector $\boldsymbol{b}_i$ and vector ${}^p\boldsymbol{p}_i$ are listed in Table. 1.

Table 1. Parameters of cubic structure of the robot.

Fixed points	Positions of Connection points on the base	Positions of onnection points on the moving platform
1	$\boldsymbol{b}_1$=$(\frac{1}{2}L, \frac{1}{2}, H)$	${}^p\boldsymbol{p}_1$=$(\frac{k_1}{2}L, \frac{k_2}{2}W, \frac{k_3}{2}H)$
2	$\boldsymbol{b}_2$=$(\frac{1}{2}L, \frac{1}{2}W, 0)$	${}^p\boldsymbol{p}_2$=$(\frac{k_1}{2}L, \frac{k_2}{2}W, -\frac{k_3}{2}H)$
3	$\boldsymbol{b}_3$=$(\frac{1}{2}L, -\frac{1}{2}W, H)$	${}^p\boldsymbol{p}_3$=$(\frac{k_1}{2}L, -\frac{k_2}{2}W, \frac{k_3}{2}H)$
4	$\boldsymbol{b}_4$=$(\frac{1}{2}L, -\frac{1}{2}W, 0)$	${}^p\boldsymbol{p}_4$=$(\frac{k_1}{2}L, -\frac{k_2}{2}W, -\frac{k_3}{2}H)$
5	$\boldsymbol{b}_5$=$(-\frac{1}{2}L, \frac{1}{2}W, H)$	${}^p\boldsymbol{p}_5$=$(-\frac{k_1}{2}L, \frac{k_2}{2}W, \frac{k_3}{2}H)$
6	$\boldsymbol{b}_6$=$(-\frac{1}{2}L, \frac{1}{2}W, 0)$	${}^p\boldsymbol{p}_6$=$(-\frac{k_1}{2}L, \frac{k_2}{2}W, -\frac{k_3}{2}H)$
7	$\boldsymbol{b}_7$=$(-\frac{1}{2}L, -\frac{1}{2}W, H)$	${}^p\boldsymbol{p}_7$=$(-\frac{k_1}{2}L, -\frac{k_2}{2}W, \frac{k_3}{2}H)$
8	$\boldsymbol{b}_8$=$(-\frac{1}{2}L, -\frac{1}{2}W, 0)$	${}^p\boldsymbol{p}_8$=$(-\frac{k_1}{2}L, -\frac{k_2}{2}W, -\frac{k_3}{2}H)$

In Eq. (7), $\Delta\boldsymbol{T}$ can be denoted as $\boldsymbol{T}_\Delta$ which balances the external wrench that satisfies $\mathbf{A}\boldsymbol{T}_\Delta = \boldsymbol{W}_{ext}$ from which it has $\boldsymbol{T}_\Delta = \mathbf{A}^{-1}\boldsymbol{W}_{ext}$, and thus the elements $T_{\Delta i}$ in $\boldsymbol{T}_\Delta$ can be obtained. From this the force and moment exerted on the moving platform can be formulated as

$$\sum_{i=1}^{m} T_{\Delta i}\boldsymbol{u}_i = \boldsymbol{f}_e \tag{8}$$

and

$$\sum_{i=1}^{m} T_{\Delta i}\boldsymbol{r}_i \times \boldsymbol{u}_i = \boldsymbol{\tau}_e \tag{9}$$

These two equations can be further written as

$$\begin{cases} \sum_{i=1}^{m} T_{\Delta i}u_{ix} = f_{ex} \\ \sum_{i=1}^{m} T_{\Delta i}u_{iy} = f_{ey} \\ \sum_{i=1}^{m} T_{\Delta i}u_{iz} = f_{ez} \end{cases} \tag{10}$$

and

$$\begin{cases} \sum_{i=1}^{m} T_{\Delta i}\left(r_{iy}\cdot u_{iz} - r_{iz}\cdot u_{iy}\right) = \tau_{ex} \\ \sum_{i=1}^{m} T_{\Delta i}\left(r_{iz}\cdot u_{ix} - r_{ix}\cdot u_{iz}\right) = \tau_{ey} \\ \sum_{i=1}^{m} T_{\Delta i}\left(r_{ix}\cdot u_{iy} - r_{iy}\cdot u_{ix}\right) = \tau_{ez} \end{cases} \tag{11}$$

Then, using the Eqs. (10) and (11) and the parameters in Table.1, the vectors $\boldsymbol{r}_i$ and $\boldsymbol{u}_i$ can be obtained and the difference $\boldsymbol{T}_\Delta$ could be calculated in terms of Eq. (7) when a constant external wrench is applied on the moving platform. In addition, sensitivity S of the CDPR can be formulated and calculated as

$$S = \sqrt{\sum_{i=1}^{m}\left(\frac{\Delta T_i}{m}\right)^2} \tag{12}$$

with $i = 1, \cdots, m$. With the same feasible algorithm for $\mathbf{A}\boldsymbol{T}_\Delta = \boldsymbol{W}_{ext}$, force sensitivity is obviously decided by the structure matrix $\mathbf{A}$ and consequently become larger if each element of the $\Delta\boldsymbol{T}$ increase. Therefore, the force sensitivity

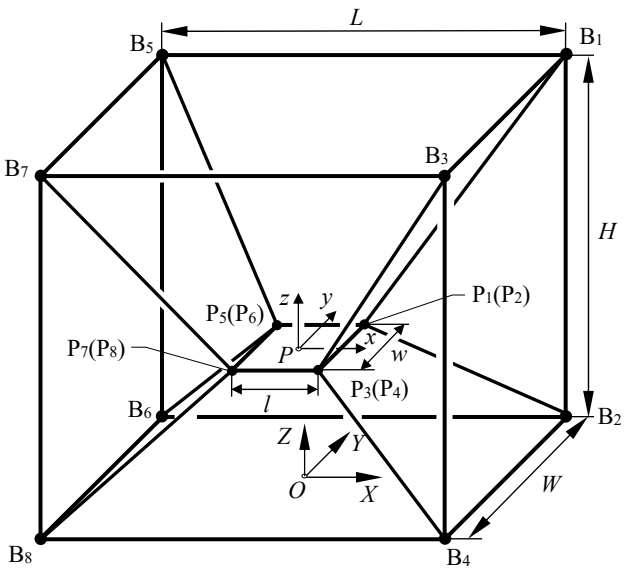

Figure 4. A 6-DOF CDPR with a flat moving platform.

of a CDPR can be determined by checking whether the following equation is solvable:

$$\text{Maximize} \qquad S(\boldsymbol{T}_\Delta, k_1, k_2, k_3)$$

$$\mathbf{s.t.} \begin{cases} \mathbf{A}\boldsymbol{T}_\Delta = \boldsymbol{W}_{ext} \\ 0.025 \le k_3 \le k_2 \le k_1 \le 0.4 \end{cases} \tag{13}$$

Thus, during the working process of CDPRs, each pose will constitute a special structure matrix which is defined by the parameters. Actually, the simultaneous equations do not have a specific expression. For this complex non-linear optimization problem, there is no effective numerical method. In order to get the result for force sensitivity with respect to the structure matrix, one method can statistically solve the problem is repeatedly changing the iterative step, and ultimately find the maximum value through contrasting each figure.

CDPR with a flat moving platform

Compared to CDPRs with cubic-shape moving platform, there are also CDPRs that have more than two of the eight cables connected at a same point on the moving platform and all these points locate on the same place [16;33;36]. In such a type of CDPRs, with the general configuration indicated in Fig. 4, each of the four attaching points on the moving platform is connected with two cables and these four points make a quadrilateral, which is named as flat moving platform. This section discuss sensitivity of a CDPR with configuration illustrated in Fig. 4. Though the moving platform can be in other shapes such as a triangle or a rhombus, the same analysis can be conducted according to the methodology proposed herein. Similar to the previous section, in order to

characterize the force sensitivity, related to the positions the eight points, two of the geometrical parameters denote as K_1 and K_2 are defined. K_1 is the ratio between length of the moving platform and length L of the supporting fram denoted as $K_1 = l/L$, and K_2 the ratio between w and W denoted as $K_2 = w/W$. The height of the base is H, it can change but there is no contrast to the moving platform f its height can be neglected. Together with position vector the reference point P in the moving platform, the geometr parameters for this case are

$$K_1 = l/L, \quad K_2 = w/W, \quad \boldsymbol{p} = [X, Y, Z]^T$$

Similarly, all these parameters can make change to the structure matrix $\mathbf{A}$ of CDPRs and thus the force sensitivity, in the case that the following equation is solvable:

$$\text{Maximize} \qquad S(\boldsymbol{T}_\Delta, \quad K_1, \quad K_2, \quad H)$$

$$\text{s.t.} \begin{cases} \mathbf{A}\boldsymbol{T}_\Delta = \boldsymbol{W}_{ext} \\ 40 \le K_1 \le K_2 \le 100 \\ 0.5 \le H \le 3 \end{cases} \tag{14}$$

Other different analysis on the CDPR with a flat moving platform is that two different algorithms for cable tension distribution would be used to identify the efficient method to find out the cable tension difference of the CDPRs, with regard to the same structure matrix $\mathbf{A}$. Although there are many algorithms for cable tension, the two algorithms mentioned above are the penalty function method and the improved closed-form method. With the same minimum and maximum values of cable tension, $\boldsymbol{T}_\Delta$ can be distinctly calculated and the force sensitivity of the CDPRs would be found out. However the challenge will be put on the control system if $\boldsymbol{T}_\Delta$ is large, which will lead to the discontinuous problem of the serve motors.

Numerical Simulation, Results and Discussions

Based on the formulation and algorithms proposed in the previous sections, in this section numerical examples are used to simulate and evaluate the feasibility of the proposed approach. In the light of the previous sections, a flowchart for calculating sensitivity of the CDPRs is presented in Fig. 5. Figure 5 depicts the details of the iterative method used to find the relationship between the geometric configuration and the external force, and thus sensitivity of the CDPRs.

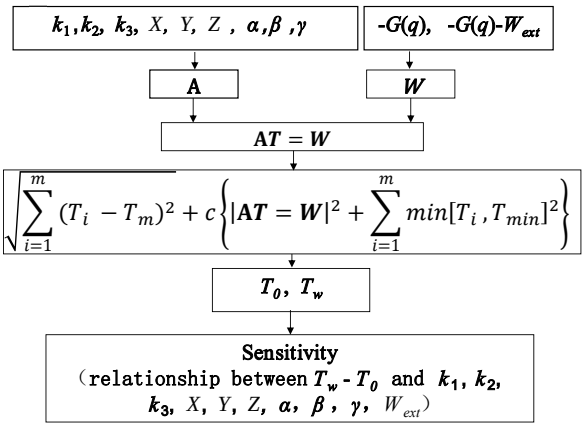

Figure 5. Flowchart for calculating the sensitivity of the CDPRs.

Numerical simulation for the CDPR with a cubic-shaped moving platform

For the CDPR with a cubic-shaped moving platform, an initial geometric configuration of the device can be obtained intuitively, which serves as a starting point to begin the dimensional determination. The architecture is presented in Figure 3 in which the dimensions of the base frame are assigned as $L = 2, W = 1.2, H = 1.4$, $\boldsymbol{p} = [0 \quad 0 \quad 0.5H]^T$ and the mass of moving platform is set as 5kg. In reality, the lower and upper tension limits are set at 35N and 1000N, respectively. For each geometric configuration, the force sensitivity is calculated when external forces are applied on three different directions according to the reference system shown in Fig. 2. The magnitudes of these external forces $\boldsymbol{f}_e$ are, respectively, 19.041N, 32.183N, 48.327N, 60.949N, 70.043N and 75.706N, which were obtained through the wind tunnel tests[16]. Then according to the configuration shown in Fig. 3 and the geometric parameters shown in Table 2, 960 times of tests were implemented on the robot. Taking some samples, Fig. 6 and Fig. 7 present the effects of difference combinations of all the cable tension on the sensitivity, computed on the external forces exerted along the x direction and y direction with respect to the geometric configurations associated with variables k_1, k_2, and k_3.

From Fig. 6(1), it can be found that the highest sensitivity for the external force along the x-axis occurs when $k_1 = 0.15$. Figure 7(1) shows that in the y-axis the sensitive configurations are decreasing, especially, the sensitivity in the case when $k_1 = 0.1$ is in the zag. This means that the geometric dimension is not suitable for testing the external force along the y-axis.

As illustrated in Fig. 6(2), concerning the geometric dimension of the width, it can be found that for the external force along the x-axis, the sensitive configurations decrease without zag, which is overwhelmingly suitable for

Table 2. Geometrical characteristics of the robot.

Geometrical configuration	$k(k_i, i = 1, 2, 3)$	Z(m)
1	0.025	
2	0.05	
3	0.075	0.1
4	0.1	0.2
5	0.125	0.3
6	0.15	0.4
7	0.175	0.5
8	0.2	0.6
9	0.225	0.7
10	0.25	0.8
11	0.275	0.9
12	0.3	1.0
13	0.325	1.1
14	0.35	1.2
15	0.375	
16	0.4	

determining the geometric dimensions. From Fig. 7(2), it can be seen that in the cases that $k_2 = 0.075$ and $k_2 = 0.3$, there exist the highest sensitivity, and there can be used for minimizing the structure of measurement device.

In Fig. 6(3) and Fig.7(3), it can be noticed that the geometric dimension of the height increases, the sensitivity of the device increases. Especially, the sensitivity is different when $k_3 = 0.05$ and $k_3 = 0.075$. The geometric dimension of the width has less influence o n t he s ensitivity f or the external force along the x-axis than that along the y-axis. In general, it can be noticed that the increase of the magnitude of the external force results in the increase of the sensitivity of the device.

The above figures s how t hat t he o ptimal geometric dimensions for length, width and height of the moving platform are $k_1 = 0.15$, $k_2 = 0.075$ and $k_3 = 0.075$ or 0.1, respectively.

Figures 8 and 9 show the sensitivity performance for the external force along the x- and y- directions of the local coordinate system, varying with respect to the Z-coordinate of the reference point P. In particular, Fig. 8 presents the sensitivity for the external force along the x-axis; it can be seen that a considerable decrease occurs in the range from Z=0.3m to Z=0.6m. The figures bottom out at Z=0.7m and there is an upward trend in the interval of Z=0.7m to Z=1.1m. The apparent consideration can be taken for the sensitivity of the external force along the y-axis, shown in Fig.9, has a distinct trend. Actually, Fig. 9 unfolds that the sensitivity not only increases with the increase of the magnitude of the external force but also with the decrease of the displacement in the Z-axis, the later means that the sensitivity increases if an outrange geometry of the device is adopted.

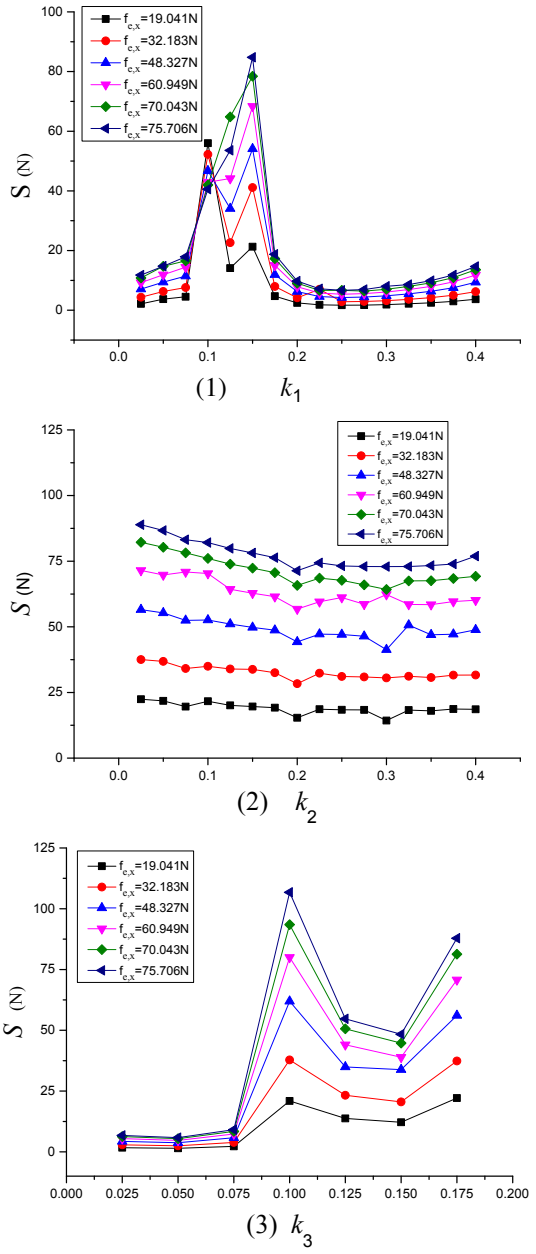

Figure 6. Sensitivity S for the external force along the x-axis (geometric dimension of the length).The plot(1) shows the value of the determinant for k_1, plot(2) shows the value of the determinant for k_2 and plot(3) shows the value of the determinant for k_3.

In the practical measurement, the vector of the external force is not invariably along the x- or y- axis. Figures 10 and 11 unfold the sensitive behavior for the highest sensitive of the unbalance external force, varying deflection distance from origin of force to the reference point P. Figure 10 shows the range of deflection distance is from -0.3m to 0.3m along the y-axis. The sensitivity is symmetry and hits the peak at the zero deflection distance, which means the test device is keenness to the external force with no deflection distance along the x-axis. Similarly, Fig. 11 has the same tendency as that indicated in Fig. 11. However it is not quintessential to the influence of the unbalance loading. These last two

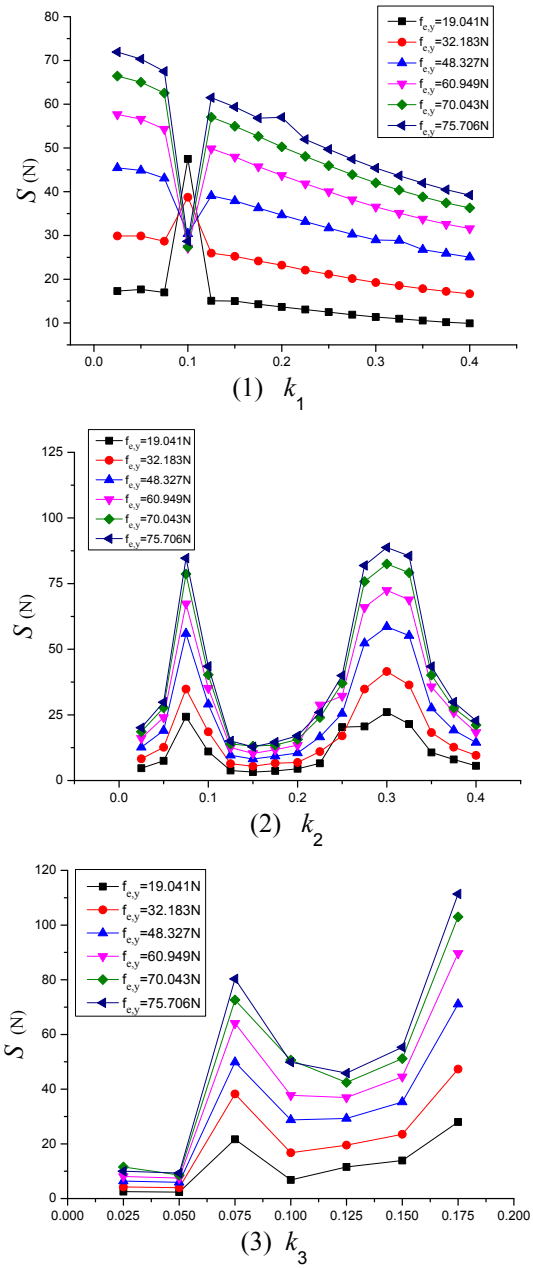

Figure 7. Sensitivity S for the external force along the y-axis (geometric dimension of the width) The plot(1) shows the value of the determinant for k_1, plot(2) shows the value of the determinant for k_2 and plot(3) shows the value of the determinant for k_3.

figures show the effective test is for the external force with no deflection displacement.

Numerical simulation for the CDPR with a flat moving platform

Follow the flowchart i n F ig. 5 , n umerical s imulation of the CDPR with a flat m oving p latform c an b e similarly conducted, while the parameters k_1, k_2 and k_3 are replaced by K_1, K_2 and H. The algorithm for identifying the cable tension includes both the penalty function method and the improved closed-form method. The upper and lower limits

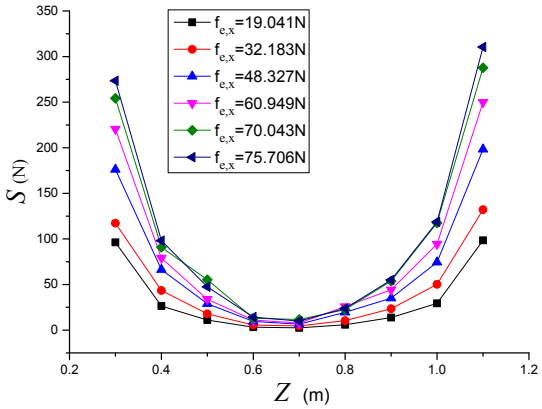

Figure 8. Values of resultant sensitivities as the external force along the x-axis applied on the moving platform when an increasing Z-coordinate of the reference point P.

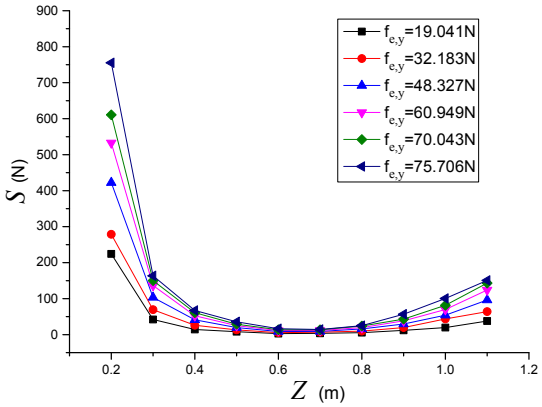

Figure 9. Values of resultant sensitivities as the external force along the y-axis applied on the moving platform with an increasing Z-coordinate of the reference point P.

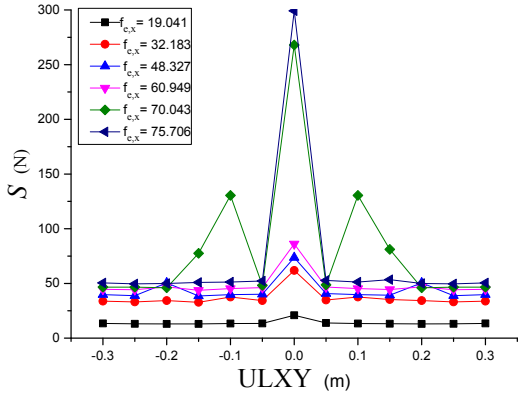

Figure 10. Values of resultant sensitivities as the external force along the y-axis applied on the moving platform with an increasing deflection with respect to the reference point P along the x-axis.

of the cable tension are set as 35N and 300N respectively, and the mass of moving platform is set as 0.64 kg. In terms of the limited space of the circumstance of the test[29], the length of the base ($L = 1m$) has restriction, which results in K_1 being constant. Further, the shape of four connected points of moving platform presented in Fig. 3 is an isosceles

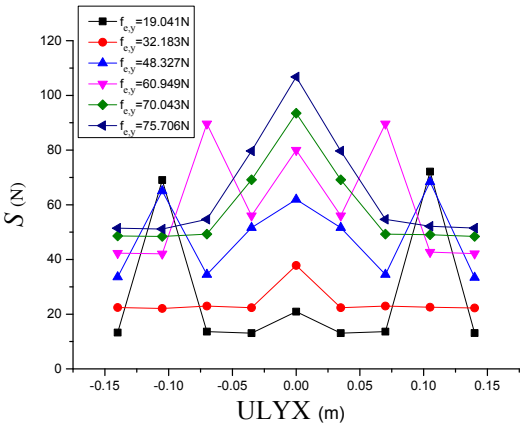

Figure 11. Values of resultant sensitivities as the external force along the x-axis applied on the moving platform with an increasing deflection with respect to the reference point P along the y-axis.

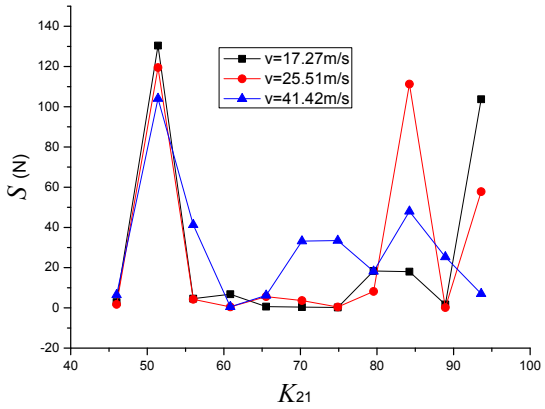

Figure 12. Values of resultant sensitivities as the external wrench applied on the moving platform with an increasing width of front base.

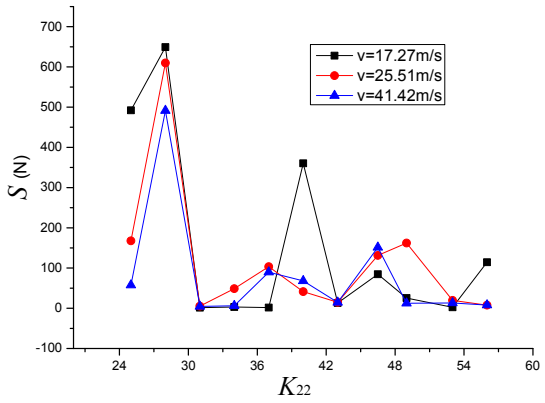

Figure 13. Values of resultant sensitivities as the external wrench applied on the moving platform with an increasing width of back base.

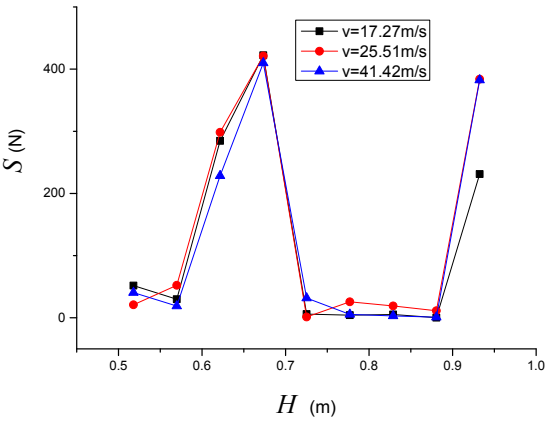

Figure 14. Values of resultant sensitivities as the external wrench applied on the moving platform with an increasing height of base.

trapezoid, which means the width, $P_5P_7 \neq P_1P_2$. Thus, the width of P_5P_7 was assigned as w_1 and the width of P_1P_2 was assigned as w_2 ($w_1 = 0.01$m and $w_2 = 0.04$m). Accordingly, the ratio K_2 was switched into $K_{21} = W/w_1$ ($W = B_1B_3$, width of front base) and $K_{22} = W/w_1 (W = B_5B_7$, width of back base). The length of moving platform is set as $l = 0.03$m and the position is set as $\boldsymbol{p} = (X, 0, 0.5H)$. The other parameters are given in Table.3 and the external wrench were calculated according to three different speeds which are 17.27 m/s, 25.51 m/s and 41.42 m/s respectively [13]. The external wrench has six components including three forces(drag, sideslip and lift) and three moments (roll, pitch and yaw). The simulation results are illustrated in Figs.12 to 15.

Table 3. Geometrical characteristics of the base.

Geometrical configuration	K_{21}	K_{22}	H(m)	X(m)
1	46	25	0.52	0.5
2	51	28	0.57	0.55
3	56	31	0.62	0.6
4	61	34	0.67	0.65
5	66	37	0.72	0.7
6	71	40	0.77	0.75
7	76	43	0.82	0.8
8	81	46	0.87	0.85
9	86	49	0.92	0.9
10	91	52		0.95
11	96	55		1

Figs.12 and 13 show that the width of the front base can be set to 0.51m($K_{21} = 51$) and the width of the back base can be set to 1.12m($K_{22} = 28$), which will significantly increase the force sensitivity. The similar effect is demonstrated at the point when $H = 0.67$m as shown in Fig.14, but there is almost non effective rewarding when the increase implemented to the coordinate value on the X-axis of the reference point P in Figs.14 and 15, which means the optimal solution for H is in the middle point of the tunnel. From the above analysis, a vital conclusion could be drawn is some parameters have no impact on the force sensitivity.

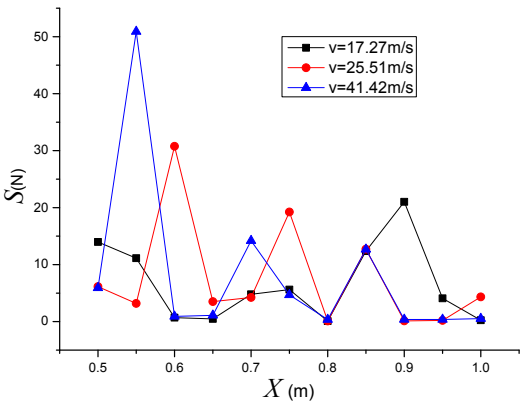

Figure 15. Values of resultant sensitivities as the external wrench applied on the moving platform with an increasing X-coordinate of the reference point P.

Figure 16. A flat moving platform inside the aircraft in the wind tunnel test.

Experiment validation

Experiments were conducted on the physical prototype, as shown in Fig.16, a CDPR consists of frame, pulleys, cables, servo motors, motion control card, monitor, transmission system, a SDM aircraft model (the fuselage diameter is 53.9 mm, the maximum length is 377.6 mm, and the wingspan is 244.1 mm), and tension sensors, as well as the vision measurement system, which uses a camera to capture the real-time pose of moving platform. The prototype with a flat platform inside the aircraft was placed in a low-speed wind tunnel. The entrance and exit ends of the tunnel are in octagonal shape, with the side length of 356 mm and 396 mm, respectively. The axial length of test section is 1075 mm. By regulating the fan speed through frequency modulator, the incoming flow speed can be adjusted in the range of 0–51 m/s. In order to monitor the actual pose of aircraft model and the cable tension, a camera and eight force sensors are used. As to the aircraft pose, six mark points are set on the surface, which would be captured by the camera through an infrared light source. After the camera calibration and image process, the position and attitude information could be derived. The measurement precision of attitude is 0.1 °, and that of position is 0.5 mm. As to the cable tension, the force sensors were set on the slide block, which moves along the ball screw.[37]

Due to the practical application, the experiments only focus on the CDPR with the flat platform inside the aircraft and was divided into two kinds of tests. One was to test the optimised parameters increasing the sensibility of the cable forces, which were $K_{21} = 51$ and $K_{22} = 28$. That meant the width of the front base was set as 0.51m and the width of the back base was set as 1.12m. By monitoring camera when the aircraft is driven by the wind, the control system keeps pose of the aircraft static in the process of moving it to another test point. Then, the stable output data from tension sensors were obtained after a short time of turbulent caused by the wind impact. Compared with the simulation results, it can be found that the maximum absolute error is about 1N, which is quite significant for the requirement in the wind tunnel test.

Another kind of test was to verify the two algorithms with the specific parameters for the non-sensibility of the cable forces. One of the set of specific parameters picked out is $K_{21} = 61$, $K_{22} = 34$, $H = 0.72$m and $x = 0.5$m and only one external force (in the case that $v = 41.42$m/s) was applied on the moving platform. In the improved close-form algorithm, the objective is to let all cables tension close to the medium at the cost of satisfying the Eq.(4). The minimum and the maximum of the cable tension is set as $T_{\min} = 35$N, and $T_{\max} = 285$N respectively, which is different with the sets above. Then the medium is $T_m = 160$N and cable tension is set within the range of 80N to 200N based on the improved close-form algorithm.

In this kind of test, all the cables tension was calculated and distributed in advance through a wide range of iterations. The cables tension collected by sensors are shown in Fig.17 and Fig.18. Since the minimum value of the cable tension under the two algorithms are clearly different, it can be found that the force sensitivity are extraordinarily manifest. However, it is formidable to make the control smoothly for the jumping value of cable tension. Moreover, it also is struggle to find the suitable difference for cable tension from two algorithms. But the methodology above mentioned are efficient for those parameters that have non sensitive to the force.

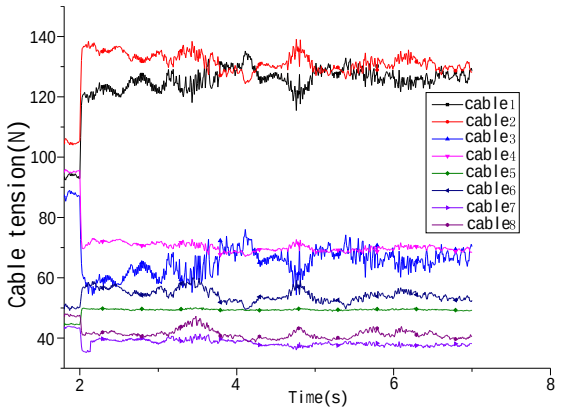

Figure 17. Values of all cable tension distributed by the penalty function with an increasing time keeping the moving platform under the constant external wrench.

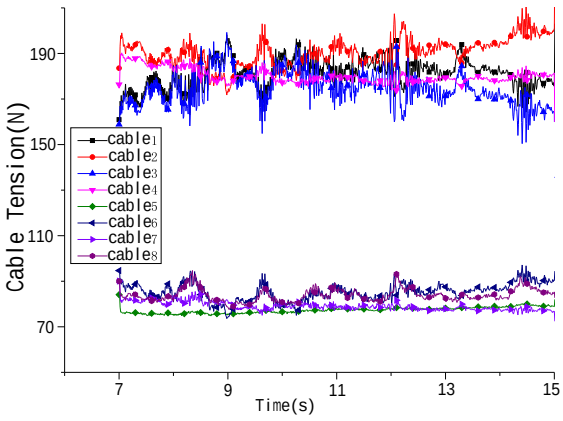

Figure 18. Values of all cable tension distributed by the improved close-form, switching from the penalty function with an increasing time keeping the moving platform under the constant external wrench.

Conclusions

This paper presented and formulated the force sensitivity of a CDPR through identifying feasible geometric dimensions. Kinematics and dynamics of the 6-DOF CDPR were derived heading to the structure matrix. Based on the structure matrix and using optimal algorithms, sensitivity of the CDPR was investigated resulting in the optimal geometric parameters for the CDPRs.

Based on the cubic moving platform, results show that the best dimensions for length, width and height of the moving platform with the promising sensitivity, are $k_1 = 0.15$, $k_2 = 0.075$ and $k_3 = 0.075$ or 0.1, respectively. The lower the location of the reference point on moving platform, the better the sensitivity for the instantaneous change of the cable tension. On top of this, the results show that the parameterising structure matrix for force sensitivity is effective. However, for the flat-type moving platform, the parameterising structure matrix is less effective than that of the cubic-shape moving platform.

Experiment validation in the wind tunnel test was carried out on the CDPR with a flat moving platform. The maximum absolute error is about 1N compared to the simulation results with the optimized parameters, which indicates that the proposed method is effective and efficient.

The modeling, analysis and sensitivity for cable tension investigated in this work hence have provided the designers with important pieces of information for choosing the best geometric parameters for developing measurement equipment based on CDPRs.

Future work will be firstly directed to verify the relationship between the stiffness and the sensitivity, which are both influenced by the geometric dimensions, positions of the hinges and cables tension. In addition, the algorithms for distribution of cables tension still need to be improved to be overwhelmingly quick to promise the real-time control of the cables tension.

Declaration of conflicting interests

The author(s) declared no potential conflicts of interest with respect to the research, authorship, and/or publication of this article.

Funding

The author(s) gratefully appreciate the financial support by the Training Program of FuJian Excellent Talents in University(FETU), the National Natural Science Foundation of China with Grant 12072304, the Scientific Research Foundation of Jimei University of China and the Application with Grant ZQ2019045 and Educational Research Projects of Young and Middle-aged Teachers in Fujian Province of China with Grant JT180267.

References

1. Tanaka M, Seguchi Y and Shimada S. Kineto-static of skycam-type wire transport system. In: Proceedings of USA-Japan Symposium on Flexible Automation, Crossing Bridges: Advances in Flexible Automation and Robotics 1998; 689-694.
2. Duan RD. Five hundred meter aperture spherical radio telescope (FAST). *Science in China* 2006; 49(2): 129-148.
3. J, Bostelman R and Dagalakis N. The NIST robocrane, *Journal of Robotic Systems* 1992;97(3):373-385.
4. Zi B, Lin J and Qian S. Localization, obstacle avoidance planning and control of a cooperative CDPR for multiple mobile cranes. *Robotics and Computer-Integrated Manufacturing* 2015; 34: 105-123.
5. Pinto AM, Moreira E, Lima J et al. A cable-driven robot for architectural constructions: a visual-guided approach for motion control and path planning. *Autonomous Robots* 2017; 41(7): 1487-1499.

6. Barnett E and Gosselin C. Large-scale 3D printing with a cable-suspended robot. *Additive Manufacturing* 2015; 7: 27-44.
7. Varela MJ, Ceccarelli M and Flores P. A kinematic characterization of human walking by using CatraSys. *Mechanism and Machine Theory* 2015; 86: 125-139.
8. Jin X, Prado A and Agrawal KA. Retraining of Human Gait - Are Lightweight Cable-Driven Leg Exoskeleton Designs Effective? *IEEE Transactions on Neural Systems and Rehabilitation Engineering* 2018; 26(4): 847-855.
9. R. Hidayah, S. Chamarthy, A. Shah, et al. Walking With Augmented Reality: A Preliminary Assessment of Visual Feedback With a Cable-Driven Active Leg Exoskeleton (C-ALEX), *IEEE Robotics and Automation Letters* 2019; 4(4):3948-3954.
10. Zanotto D, Rosati G. Minto S, et al. Sophia-3: a semiadaptive cable-driven rehabilitation device with tilting working plane. *IEEE Transactions on Robotics* 2014; 30(4): 974-979.
11. Mao Y, Jin X, Dutta GG, et al. Human movement trainign with cable driven arm exoskeleton (CAREX). *IEEE Transactions on Neural Systems and Rehabilitation Engineering* 2015; 23(1): 84-92.
12. Martelli D, Luo L, Kang J et al. Adaptation of stability during perturbed walking in Parkinson's disease. *Scientific Reports* 2017; 7: 17875.
13. Xiao YW, Lin Q, Zheng YQ, et al. Model aerodynamic tests with a wire-driven parallel suspension system in low-speed wind tunnel. *Chinese Journal of Aeronautics* 2010; 23(4): 393-400.
14. Bruckmann T, Hiller M and Schramm D. An active suspension system for simulation of ship maneuvres in wind tunnels. In: Pisla D., Ceccarelli M., Husty M., Corves B. (eds) *New Trends in Mechanism Science. Mechanisms and Machine Science* 2010; 5: 537-544, Springer, Dordrecht.
15. Magill JC, Cataldi P, Morency JR et al. Demonstration of a Wire Suspension for Wind-Tunnel Virtual Flight Testing. *Journal of Spacecraft and Rockets* 2012; 46(3): 624-633.
16. Wang X, Peng M, Hu Z, et al. Feasibility investigation of large-scale model suspended by cable-driven parallel robot in hypersonic wind tunnel test. *Proceedings of the Institution of Mechanical Engineers, Part G: Journal of Aerospace Engineering* 2017; 231(13): 2375–2383.
17. Abdolshah S and Rosati G. Improving performance of cable robots by adaptively changing minimum tension in cables. *International Journal of Precision Engineering and Manufacturing* 2017; 18(5): 673-680.
18. Gouttefarde M, Lamaury J, Reichert C, et al. A versatile tension distribution algorithm for n-DOF parallel robots driven by n+2 cables. *IEEE Transactions on Robotics* 2015; 31(6): 1444-1457.
19. Pott A. An improved force distribution algorithm for over-constrained cable-driven parallel robots. In: Thomas F, Perez Gracia A (eds) Computational Kinematics. *Mechanisms and Machine Science* 2014; 15: 139-146, Springer, Dordrecht.
20. Boumann R, Bruckmann T. Computationally Efficient Cable Force Calculation Outside the Wrench-Feasible Workspace. In: Kuo CH, Lin PC, Essomba T, Chen GC. (eds) Robotics and Mechatronics. ISRM 2019. *Mechanisms and Machine Science* 2020; 78: 177-188, Springer Cham.
21. Dai JS and Kerr DR. A six-component contact force measurement device based on the Stewart platform, *Proceedings of the Institution of Mechanical Engineers, Part C: Journal of Mechanical Engineering Science* 2000; 214(5):687-697.
22. Mura A. Sensitivity analysis of a six degrees of freedom displacement measuring device. *Proceedings of the Institution of Mechanical Engineers Part C: Journal of Mechanical Engineering Science* 2014; 228(1): 158-168.
23. Gianni Di P and Stefano L. An Augmented Lagrangian Function with Improved Exactness Properties. *SIAM Journal on Optimization* 2002; 12(2): 376-406.
24. Su YX and Duan BY. The application of the Stewart platform in large spherical radio telescopes. *Journal of Robotic Systems* 2000;17(7):375-83.
25. Gosselin C and Grenier M. On the determination of the force distribution in overconstrained cable-driven parallel mechanisms. *Meccanica* 2011;46(1):3-15.
26. Hiller M, Fang S, Mielczarek S, et al. Design, analysis and realization of tendon-based parallel manipulators. *Mechanism and Machine Theory* 2005;40(4):429-45.
27. Bruckmann T, Pott A and Hiller M. Calculating force distributions for redundantly actuated tendon-based Stewart platforms. In: *Advances in Robot Kinematics: Mechanisms and Motion* Dordrecht, Springer, 2006. pp. 403-12.
28. Wang X, Ma S and Lin Q. Hybrid pose/tension control based on stiffness optimization of cable-driven parallel mechanism in wind tunnel test. In:*2nd International Conference on Control, Automation and Robotics (ICCAR)*, Hong Kong, China, 28-30 April 2016.pp. 75-79.
29. MING A and HIGUCHI T. Study on multiple degree of freedom positioning mechanisms using wires (Part 1)conceptdesign and control. *International Journal of the Japan Society for Precision Engineering* 1994;28(2):131-138.
30. Fang S, Franitza D, Torlo M, et al. Motion control of a tendon-based parallel manipulator using optimal tension distribution. *IEEE/ASME Transactions on Mechatronics* 2004;9(3):561-568.
31. Borgstrom PH, Jordan BL, Sukhatme G, et al. Rapid Computation of Optimally Safe Tension Distributions for Parallel Cable-Driven Robots. *IEEE Transaction on Robotics*

2009;25(6):1271-1281.

32. Gosselin C and Grenier M. On the determination of the force distribution in over constrained cable-driven parallel mechanisms. *Meccanica* 2011;46(1):3-15.
33. Hassan M and Khajepour A. Analysis of Bounded Cable Tensions in Cable-Actuated Parallel Manipulators. *IEEE Transaction on Robotics* 2011;27(5):891-900.
34. Abbas F and Sunil KA. On the Design of Cable-Suspended Planar Parallel Robots. *Journal of Mechanical Design* 2005; 127(5): 1021-1028.
35. Perreault S and Clement MG. Cable-Driven Parallel Mechanisms: Application to a Locomotion Interface. *Journal of Mechanical Design* 2008;130(10):102301:1-8.
36. Pott A and Schmidt V. On the Forward Kinematics of Cable-Driven Parallel Robots. *IEEE/Rsj International Conference on Intelligent Robots and Systems. IEEE International Conference on Intelligent Robots and Systems* Hamburg, Germany, 28 Sep.-2 Oct. 2015. p. 3182-3187.
37. Wang, X., Hu, Y., and Lin, Q. Workspace analysis and verification of cable-driven parallel mechanism for wind tunnel test. *Proceedings of the Institution of Mechanical Engineers. Part G, Journal of aerospace engineering* 2017; 231(6): 1012-1021.

Appendix

Nomenclature

α	the roll angle
β	the yaw angle
$\boldsymbol{\tau}_e$	the external force
$\boldsymbol{\tau}_e$	the external moment
$\boldsymbol{a}_i$	element of the Jacobean matrix
$\boldsymbol{b}_i$	the position vector of the point -shaped hinge in the global coordinate system
$\boldsymbol{c}$	the position vector of the centre of mass of the moving platform
$\boldsymbol{l}_i$	the vector of the *i*th cable
$\boldsymbol{p}$	the position vector of the reference point P in the global coordinate system $\{\mathrm{O}\}$
$\boldsymbol{p}_i$	the position vector of the P_i in the globe coordinate system
$\boldsymbol{q}$	the pose of the moving platform
$\boldsymbol{T}$	the vector of cable tensions
$\boldsymbol{T}_0$	the spatial force system of the cable tension to balance the gravity
$\boldsymbol{T}_w$	the spatial force system of the cable tension to balance the gravity and the external wrench
$\boldsymbol{u}_i$	the unit direction vector of the *i*th cable
$\boldsymbol{W}$	the wrench exerted on the moving platform
$\Delta\boldsymbol{T}$	the difference of the cable tension to balance with no external wrench and with external wrench
$\dot{\boldsymbol{L}}$	the velocity vector in cable length space
$\dot{\boldsymbol{q}}$	the Cartesian velocity of the moving platform
γ	the pitch angle
$\mathbf{A}$	the Jacobean matrix
$\mathbf{C}(\boldsymbol{q},\dot{\boldsymbol{q}})\dot{\boldsymbol{q}}$	the centrifugal and Coriolis force vector
$\mathbf{G}(\boldsymbol{q})$	the gravitational vector
$\mathbf{M}(\boldsymbol{q}$	the mass inertia matrix of the moving platform
$\mathbf{W}_{ext}(\boldsymbol{q})$	the external wrench
$\mathbf{0}_{3\times3}$	the zero matrix
$\mathbf{I}_{3\times3}$	the identity matrix
$\mathbf{I}_G$	the inertia tensor
$\mathbf{R}$	the rotational transformation matrix
$\{O\}$	the global coordinate system
$\{P\}$	the local coordinate system
${}^p\boldsymbol{p}_i$	the position vector of the P_i in the local coordinate system
H	the heigt of the base relate to the flat-type moving platform
k_1	the ratio of length between the cubic moving platform and base
k_2	the ratio of width between the cubic moving platform and base
k_3	the ratio of heigth between the cubic moving platform and base
K_1	the ratio of the length between the plat-type of the moving platform and base
K_{21}	the ratio of width between the flat-type moving platform and front base

K_{22} the ratio of width between the flat-type moving platform and back base

K_2 the ratio of the width between the plat-type of the moving platform and base

m_c The mass of the object

P_i the connection point of cable and moving platform

S sensitivity of the CDPR

T_m the midium cable tension

$T_{\max}$ the maximum cable tension

$T_{\min}$ the minimum cable tension